Near-inertial wave propagation in the deep Canadian Basin: Turning depths and the homogeneous deep layer

Joel Bracamontes-Ramírez[1], Maren Walter[1], Martin Losch[2]

[1]Institute of Environmental Physics, University of Bremen
[2]Alfred-Wegener-Institut, Helmholtz-Zentrum für Polar- und Meeresforschung

Key Points:

- In the deep Canadian Basin, there are near-inertial turning depths between 100 to 1200 m above the seafloor.
- Below the turning depths, the deep layer is quasi-homogeneous and locally unstable.
- Near-inertial turning depths inhibit internal gravity wave propagation and hence reduce near bottom mixing.

Corresponding author: Joel Bracamontes-Ramírez, `joelbra.92@gmail.com`

Abstract

The internal wave climate in the deep Arctic Ocean, away from the shelves, is quiet because the ice cover shields the ocean from wind energy input, and tidal amplitudes are small. Hence, mixing due to internal wave breaking is small. The shrinking Arctic sea ice cover, however, exposes more open ocean areas to energy transfer by wind. Consequently, more energetic near-inertial internal waves (NIWs) may carry energy to the bottom, potentially enhancing deep mixing. In the deep Canadian Basin, weakly stratified layers with local buoyancy frequencies smaller than the wave frequency may prevent NIW propagation to the seafloor. We estimate the distribution of these near-inertial turning depths from temperature and salinity data of the years 2005 to 2014. Near-inertial turning depths are ubiquitous in the deep Canadian Basin at ~ 2750 m depth, between 100 and 1200 m above the bottom. A deep homogeneous layer below 3300 m is characterized by small squared buoyancy frequencies $N^2 \sim 0$ with locally unstable layers ($N^2 < 0$). The turning depths reflect NIWs and hence limit their contribution to deep mixing, but the waves create an evanescent perturbation with exponentially decreasing amplitude that can interact with the bathymetry, especially above slopes and ridges where the height of the turning depths above the seafloor is small. After reflection, the main part of the wave energy is trapped between turning depths and the surface, so that a potential increase of wave energy input mainly affects mixing of mid-depth water masses like the Atlantic Water.

Plain Language Summary

Over the last couple of years, Arctic Ocean summer sea ice has decreased. The larger ice-free regions imply more open areas for wind to act on the ocean surface. As a result, energy from the atmosphere goes into the ocean, triggering more energetic waves in the ocean interior. These internal waves carry energy over longer distances and mix the waters where they break. To better understand this process, we studied temperature and salinity data from 2005 to 2014. Our findings show widespread areas in the deep Canadian Basin, at around 2750 m depth, where the further propagation of the waves is constrained by weak stratification. These depths are called near-inertial turning depths, and they shorten the path of near-inertial waves and isolate the bottom from waves and mixing. In addition, we found weakly stratified and unstable layers below 3300 m. Our results shed light on the link of surface-generate waves to the interior mixing rates in the Arctic Ocean.

1 Introduction

The energy associated with the internal wave climate in the Arctic Ocean is lower than in other oceans (D'Asaro & Morehead, 1991; Morison et al., 1985), partly because a thick sea ice layer covers the ocean surface, preventing the wind from acting on it. The ice cover varies non-uniformly in both time and space. In the marginal zone and towards the coast, the sea ice has a seasonal cycle, with thinner sea ice that usually does not survive the summer (Walsh et al., 2017). In contrast, the sea ice is thicker at higher latitudes and can survive several years (Kwok, 2018). This sea ice pattern is changing. In the last decades, the summer ice cover has decreased considerably, which implies more open ocean areas where the wind can act on and transfer energy and momentum into the ocean (Rainville et al., 2011; Rainville & Woodgate, 2009). In particular, an increase in near-inertial wave amplitude (Dosser et al., 2014; Dosser & Rainville, 2016) and kinetic energy (Fine & Cole, 2022) in the Canadian Basin and the enhancement of wind-driven vertical heat fluxes and dissipation rates in the Eurasian Basin (Meyer et al., 2017; Peterson et al., 2017) have already been observed.

Furthermore, tidal energy is weak, partly because most of the Arctic Ocean lies north of the critical latitude for the M_2 tide at 74.5 °N. North of this latitude, semi-diurnal tides cannot propagate freely but they can transfer energy into lee waves by non-linear interaction with the topography (Vlasenko et al., 2003). This process is more likely to be triggered on steep slopes, and typically lee waves tend to be dissipated near their generation zone (Rippeth et al., 2017; Lenn et al., 2022), providing another explanation that the Arctic Ocean has a quiescent wave climate.

As the summer sea ice extent continues to decrease and the areas with seasonal sea ice cover increase, wind-driven internal waves will be more energetic, mainly in the near-inertial range (Rainville & Woodgate, 2009; Rainville et al., 2011). This shift in ice cover dynamics and the fact that most of the Arctic Ocean is located north of the M_2 critical latitude make the near-inertial waves (NIW) an important contributor to altering the wave climate. In a fully sea-ice-covered Arctic Ocean, near-inertial internal waves generated at the surface are hypothesized to survive one round-trip to the bottom and then dissipate partially under sea ice (Pinkel, 2005; Cole et al., 2018). In a feasible, less dissipative future scenario with more open ocean areas (Kim et al., 2023), we expect surface-generated NIWs to travel and carry energy over longer distances towards the slope or the bottom.

As NIWs travel through the Ocean, they can reach depths at which their frequency ω exceeds the local buoyancy frequency $N(z)$ and where they cannot propagate any further as waves (Olbers, 2012). According to linear theory and experiments, waves are more likely to be reflected at these so-called turning depths than to penetrate this depth or break (Paoletti & Swinney, 2012). Hence, the NIW travel path to the surface is shortened after reflection at turning depths. Below a turning depth, wave amplitudes decrease exponentially in what is known as the evanescent region (Sutherland, 2010). Hence if turning depths are far above the topography, waves are unlikely to interact with the bottom (Paoletti et al., 2014) and to account directly for deep mixing.

Turning depths for the semidiurnal tide, with $N(z) \leq \omega_{M_2} \approx 1.405 \times 10^{-4}\,\mathrm{s}^{-1}$ ($N^2(z) \leq 1.974\times10^{-8}\,\mathrm{s}^{-2}$), are ubiquitous in the entire Ocean (King et al., 2012). In the South China Sea, turning depths were also found for the diurnal tide $\omega_{K_1} \approx 7.292\times 10^{-5}\,\mathrm{s}^{-1}$ ($\omega_{K_1}^2 \approx 0.5317 \times 10^{-8}\,\mathrm{s}^{-2}$) (Liu et al., 2022). For NIWs, the buoyancy frequency must be in the order of $N(z) \leq \omega \approx 1.4\times10^{-4}\,\mathrm{s}^{-1}$ ($N^2(z) \leq 1.959\times10^{-8}\,\mathrm{s}^{-2}$), which corresponds to the average Coriolis frequency in the Arctic Ocean ($> 70\,°$N). Such a weak stratification is found mainly at great depths, for example, in the abyssal plain of the Canadian Basin below $\sim 2700\,\mathrm{m}$ (Timmermans et al., 2007; Timmermans & Garrett, 2006). In addition, in the Canadian Basin interior, away from the continental slopes, upward and downward NIW energy fluxes at the surface dominate (Halle, 2003; Pinkel, 2005) even though the weak tides do not generate strong upward internal waves. A possible explanation without observational evidence for this upward wave flux paradox is that surface-generated NIWs reflect after encountering a turning depth in the interior (Gregg, 2021).

In the Canadian Basin, deep mixing is enhanced on slopes, particularly in areas with steep topography (Rainville & Winsor, 2008). If tides do not play a significant role in driving the mixing interior beyond the critical latitude, the pathways of NIWs are key to understanding the mechanisms that drive deep mixing in the Canadian Basin. Do near-inertial turning depths exist in the Deep Canadian Basin? Do surface-generated NIWs reach the bottom? What are the consequences of turning depths for deep mixing?

In this paper, we use temperature and salinity profiles from the Canadian Basin to investigate the existence and distribution of near-inertial turning depths in the interior and to characterize the deep homogeneous layer. Section 2 describes data and methods. Section 3 gives evidence and distribution of near-inertial turning depths, and we explored the effect of the non-traditional approximation on the detection of near-inertial

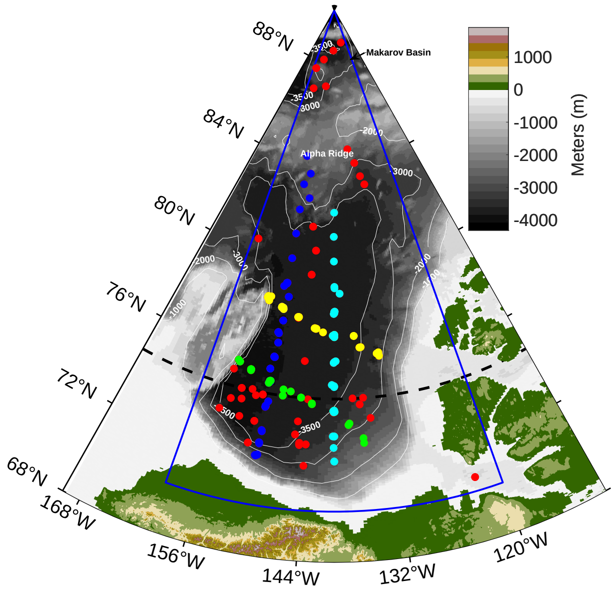

Figure 1. Canadian Basin bathymetry, the blue sector marks the study area. The dotted black line represents the critical latitude for the M_2 tide and the dots are the location of the 196 profiles used for this study. In light and dark blue, yellow, and green the profiles used for the transects shown in Fig. 4.

turning depths. Section 4 discusses the results and gives some insights into the consequence of near-inertial turning depths with a focus on mixing. Finally, the main contributions of this study are summarized in Section 5.

2 Data and Methods

2.1 UDASH temperature and salinity profiles

The Unified Database for Arctic and Subarctic Hydrography (UDASH) consists of over 250 000 high-quality temperature and salinity profiles from the Arctic and Subarctic region for latitudes north of 65° N for the period 1980 to 2015. These data were measured by conductivity-temperature-depth devices (CTDs), expendable CTDs, drifting buoys, profiling floats, and expendable, digital, and mechanical bathythermographs (Behrendt et al., 2017; Behrendt et al., 2018). The mean vertical resolution of the data is 1.5 m but varies due to the range of instrumental sources between 1 cm and 693 m. In this study, we analyzed all available 21 748 profiles of temperature and salinity within the Canadian Basin, which corresponds to 10 years of data from 2005 to 2014 for the region between the 120° W and 160° W meridians and north of 70° N. Only 196 profiles (Fig. 1) were deep enough to have a value at some depth where $N(z)^2 \leq f^2$ (see Section 3). These profiles represent only 0.9 % of the available data, and all are CTD casts, with precision and accuracy ranges of 0.02–0.001 °C and 0.002-0.0003 S/m for temperature and conductivity.

2.2 IBCAO bathymetry

The International Bathymetric Chart of the Arctic Ocean (IBCAO) Version 3.0 has a spatial grid resolution of 500 m. We computed the representative depth for each profile as an average of the nearest bathymetric data points (Jakobsson et al., 2012).

2.3 N^2_{bin} computation and near-inertial turning depths

The deep Canadian Basin is weakly stratified with small N^2 between $\sim 10^{-8} - 10^{-7}\,\mathrm{s}^{-2}$. As a consequence, the noise in the estimated N^2 is in the same order as the relatively small Coriolis frequencies f^2 ($1.87 - 2.12 \times 10^{-8}\,\mathrm{s}^{-2}$ for $70 - 90°$N), and the semidiurnal M_2 tidal frequency of ω_{M_2} ($\omega^2_{M_2} = 1.974 \times 10^{-8}\,\mathrm{s}^{-2}$). For the determination of turning depths, it is therefore important to minimize the noise in the N^2 estimation. To do so, we followed the methodology of King et al. (2012).

This method reduces the noise by taking vertical averages of the data over depth bins. King et al. (2012) found that a 100 m-bin is the optimal vertical width for averaging as the bin is wide enough to reduce the noise and narrow enough to preserve the N^2 information. Observations in the upper layers of the Canadian Basin show upward- and downward-wave energy flux with a peak within the near-inertial frequencies at vertical wavelengths of 30–50 m (D'Asaro & Morehead, 1991; Halle, 2003; Fer, 2014). Hence, the 100 m-bin width may be too large to identify turning depths for NIWs in the upper layers, or in general to study wave motions with similar or smaller vertical scales O($\leq$100 m) since the background of N^2 associated with the vertical scales in which these waves propagate is smoothed (van Haren & Millot, 2006; Ghaemsaidi et al., 2016). However, we expect NIWs will encounter a deep turning depth close to the bottom where N^2 is weak. For traveling waves, the vertical wavelength increases as N^2 decreases. We can use the following equation (Olbers, 2012), in which m and K_h are the vertical and the horizontal wavenumbers, to calculate changes in the vertical wavelength of surface-generated NIWs as they approach the bottom and roughly estimate whether a 100 m-bin is appropriate for finding turning depths for NIWs.

$$m(z) = \pm K_h \sqrt{\frac{N^2(z) - \omega^2}{\omega^2 - f^2}} \tag{1}$$

Using Eq. 1, we estimated K_h at the surface as a function of observed vertical wavelengths, 30–50 m, and $N = 8.73\times10^{-3}\,\mathrm{s}^{-1}$ (5 c.p.h.). N was computed from our dataset as an average buoyancy frequency below the pycnocline. The value is consistent with previous estimates (Cole et al., 2018; Pinkel, 2005). Assuming a wave frequency $\omega = 1.05\,f$, we obtained a horizontal wavenumber $K_h = 0.105 - 6.706 \times 10^{-4}\,m^{-1}$, which is equivalent to wavelengths of 5–10 km. These wavelengths are within the values expected for the Arctic Ocean and are also within the order of the Rossby radius of deformation (Nurser & Bacon, 2014). Therefore, we used this K_h to compute m at 1000 m, a depth 1500 m well above $N \to \omega$ (where Eq. 1 no longer applies). At this depth, $N \approx 1.03\times10^{-3}\,\mathrm{s}^{-1}$ (e.g., see in Fig. 2) and the vertical wavelengths increase from 30–50 m to 230–400 m. These vertical wavelengths are larger than 100 m, and they still increase as they approach the bottom and N continues to decrease with depth. Therefore, we argue that the 100 m-bin averaging scale is appropriate for detecting turning depths in the deep Canadian Basin in case surface-generated NIWs with vertical wavelengths of 30–50 m propagate to the bottom.

Prior to binning, in-situ temperature and salinity data was converted to conservative temperature (Θ) and absolute salinity (S_A) (McDougall & Barker, 2014, 2011). The profiles were vertically averaged in 100 m-depth bins (Θ_{bin}, $S_{A\,bin}$) and spline fitted ($\langle\Theta\rangle$, $\langle S_A\rangle$) to their respective original depths. We utilized both $\langle\Theta\rangle$ and $\langle S_A\rangle$, and the original profiles Θ and S_A, to calculate the experimental standard deviation of the mean (σ_Θ and σ_{S_A}). Subsequently, we employed a Monte Carlo method to generate an ensemble of 500 synthetic profiles by adding random Gaussian noise with a half-width of σ_Θ and σ_{S_A} to Θ_{bin} and $S_{A\mathrm{bin}}$. These ensembles were then used to compute the final averaged value of N^2_{bin} in 100 m-bins, along with its experimental standard deviation σ_{N^2} of the mean (King et al., 2012).

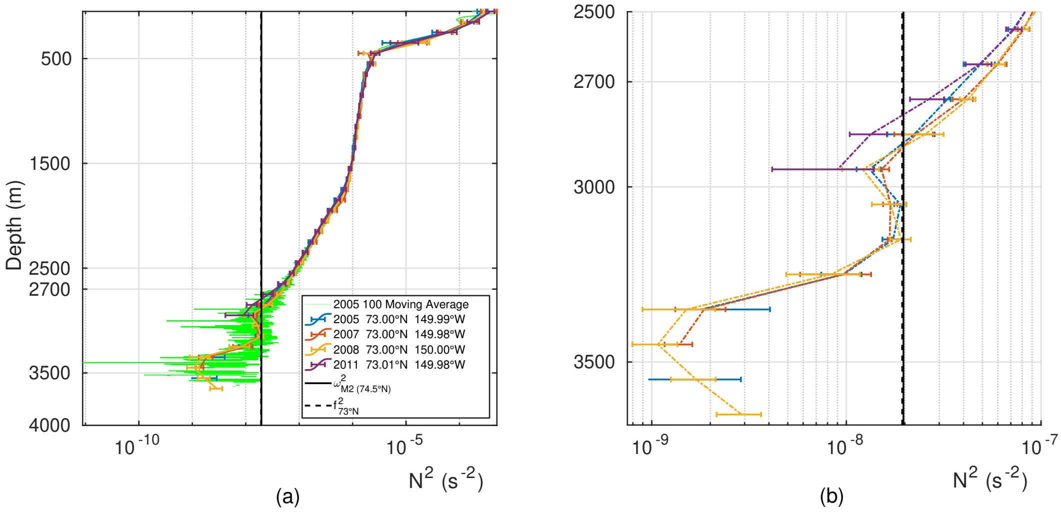

Figure 2. N^2_{bin} profiles from a small geographical region show low temporal variability between 2005 and 2011. Below 2950 m, N^2 is generally smaller than $f^2_{73^\circ N}$ and ω^2_{m2}. (a) 100 m-N^2_{bin}. (b) Zoom in to 100 m-N^2_{bin} for depths below 2500 m. In (a), the green line is the N^2_{mvg} profile, computed conventionally from smoothed hydrography from 2005 (100 m-moving-average) for comparison, see text for the details. The vertical lines indicate the frequencies for ω^2_{m2} and $f^2_{73^\circ N}$. In (a), and (b) the horizontal bars are the uncertainties σ_{N^2}.

We identified depths where $N^2_{bin}(z) \leq f^2_\phi$, in which $f_\phi = 2\Omega\sin(\phi)$, and ϕ is the latitude of each profile. This criterion defines turning depths for waves with $f_\phi \leq \omega$, which is what we expect for surface-generated near-inertial waves. In particular, we are interested in regions where there are consecutive depths $N^2_{bin}(z) \leq f^2_\phi$. Note that we used N^2_{bin} rather than N_{bin} to handle instabilities with $N^2_{bin} < 0$.

3 Results

3.1 Testing the computation of N^2_{bin}: a turning depth example

Especially at great depths, where the stratification is weak and N^2 is small, noisy θ and S_A profiles make identifying turning depths difficult. As an example of how the post-processed N^2_{bin} profiles improve this situation, we chose four profiles close to the same location at $\sim$(73 °N, 150 °W), but from different years (2005, 2007, 2008, and 2011) to illustrate the temporal (interannual) variability. In addition, and only for illustration purposes, we compare the N^2_{bin} profiles to N^2_{mvg} computed from original Θ and S_A profiles of 2005 that have been smoothed by a 100 m-moving-average.

The temporal (interannual) variability of the N^2_{bin} profiles is small (Fig. 2a) below 1000 m ($RMS_{N^2} = 6.83 \times 10^{-7}\,\mathrm{s}^{-2}$). Below 2500 m, N^2_{bin} approaches the local Coriolis frequency at 73 °N (the location of these profiles) and the tidal frequency $\omega^2_{M_2}$. These frequencies nearly coincide, because the critical latitude for the M_2 tide is at $\sim$74.5 °N (Rippeth et al., 2017). N^2_{bin} decreases further until the deep homogeneous bottom layer is reached, at $\sim$2700 m, where $N^2_{bin} \lesssim 4 \times 10^{-8}\,\mathrm{s}^{-2}$. The following consecutive depths satisfy the criterion $N^2_{bin}(z) \leq f^2_o$. In contrast, N^2_{mvg} fluctuates around f^2_ϕ (Fig. 2a) so that a turning depth cannot be identified in a statistically robust way. Note that all profiles have a very similar structure, implying that the post-processing method extracts the persistent modes of the water mass structure and does not introduce artifacts.

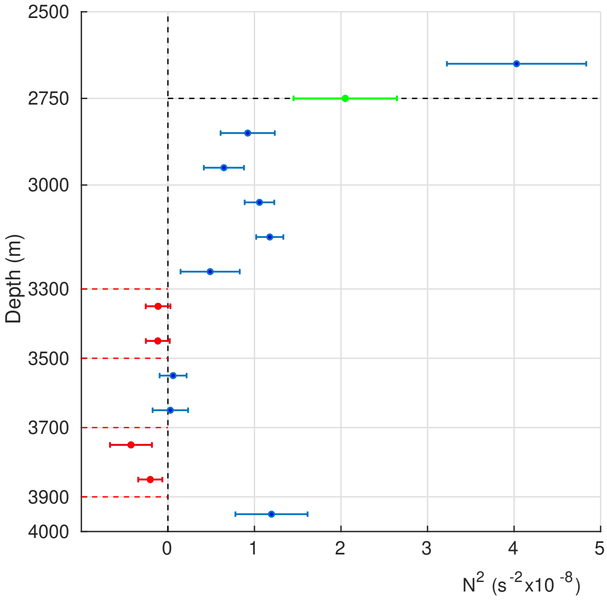

Figure 3. Averaged values of all profiles per depth for N_{bin}^2 and uncertainties σ_{N^2}. Near-inertial turning depth (NiTD) for the Canadian Basin at ∼2750 m (green dot). Evidence of locally statistically unstable layers at two depths (red dots), within 3300–3500 m and 3700–3900 m. Layers between 3700–3900 m are statistically unstable since $N_{bin}^2 + \sigma_{N^2} < 0$.

3.2 Mean N_{bin}^2 and uncertainties σ_{N^2}

Near a turning depth, $N_{bin}^2 \approx f_\phi^2$ so that, if σ_{N^2} is too large, there can be cases for which $N_{bin}^2 + \sigma_N^2 > f_\phi^2 > N_{bin}^2$. We exclude these cases and, as a condition that takes into account the estimated uncertainties, identify turning depths only if $N_{bin}^2 + \sigma_N^2 < f_\phi^2$. For instance, although below 2800 m nearly all $N_{bin}^2 \leq f_\phi^2$, there are few data for which $N_{bin}^2 + \sigma_N^2 > f_o^2$ (Fig. 2b). These will not be termed turning depths, but only the following depths for which $N_{bin}^2 + \sigma_N^2 < f_o^2$.

$N_{bin}^2 \pm \sigma_{N^2} < f_\phi^2$ or $> f_\phi^2$ varies between profiles and depths. On average, however, $N_{bin}^2 \leq f_\phi^2$ and σ_{N^2} is small (Fig. 3), so that we can apply a cumulative frequency analysis to assess the occurrence of depths where $N_{bin}^2 + \sigma_N^2 < f_o^2$. We normalized N_{bin}^2 and σ_{N^2} by f_ϕ^2, because the ratio N_{bin}^2/f_ϕ^2 is useful to define transitions between regions (green and red dotted lines in Fig. 3 and 4). We found that below 2700 m the frequency of occurrence for $(N_{bin}^2 + \sigma_N^2)/f_\phi^2 \leq 1$ is higher than 90%, which is a robust result. There is not only one 100 m-thick sporadic turning depth, but below the first depth at which $N^2 + \sigma^2 < f_\phi^2$, the stratification of the consecutive depths is also $< f_\phi^2$. Thus, the turning depth is not only a single location but a layer, making wave propagation less probable than having a single 100 m-thick turning depth value.

On average, the deep Canadian Basin is characterized by values of the ratio $N_{bin}^2/f_\phi^2 < 1$ with small uncertainties $\sigma_{N^2} \leq 0.3\, f_\phi^2$. Particularly at 2750 m, $\sigma_{N^2} \approx 0.29\, f_\phi^2$ and $N_{bin}^2/f_\phi^2 \approx 1$, so that at this depth the mean value of N_{bin}^2 is comparable to the local Coriolis frequencies within uncertainties σ_{N^2}. Hence, we identified 2750 m as the statistical near-inertial turning depth (NiTD) for the Canadian Basin.

Below 3150 m, N_{bin}^2 alternates between positive and negative values every 200 m (values between red lines in Fig. 3) suggesting locally stable ($N_{bin}^2 > 0$) and unstable ($N_{bin}^2 < 0$) layers within the (quasi-)homogeneous layer that extends to the bottom.

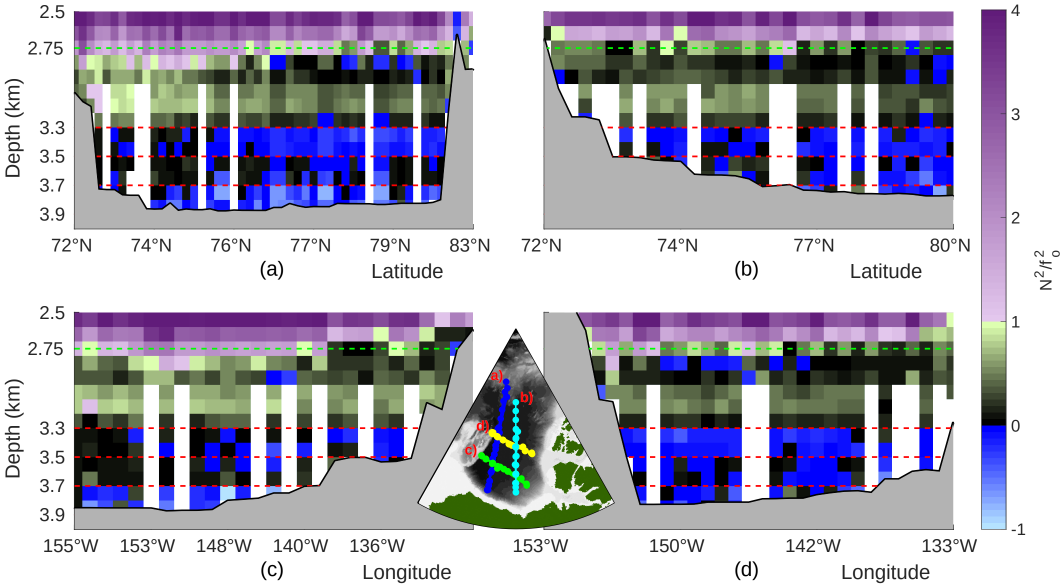

Figure 4. Ratio N^2_{bin}/f^2_ϕ for two zonal and two meridional transects in the Canadian Basin. Refer to Fig. 1 for the location of the sections: (a) Meridional section (dark blue dots in inset, cf. Fig. 1), (b) Meridional section (light blue dots), (c) Zonal section (green dots), (d) Zonal section (yellow dots). The color change from light lilac to light green defines the transition from $N^2 \geq f^2_\phi$ to $N^2 \leq f^2_\phi$. Near-inertial turning depth at ∼2750 m (green dashed line) defined by mean N^2_{bin} in Fig. 3. The color change from dark green to dark blue defines the transition from $N^2 \geq 0$ to $N^2 \leq 0$. The inset shows each transect. Evidence of locally statistically unstable layers below 3300 m. The red dotted lines refer to the unstable layers within 3300–3500 m and 3700–3900 m defined by average N^2_{bin} in Fig. 3.

Note that, between depths of 3550–4450 m, $N^2_{bin} + \sigma^2_N > 0$, hence strictly speaking, these layers are not unstable. In contrast, the layers between 3750–3850 m are locally unstable since $N^2_{bin} + \sigma^2_N < 0$. Geothermal heat fluxes from the seafloor (Timmermans et al., 2003) may trigger instability. Alternatively, since the homogeneous layer has neutral buoyancy stability, meaning that $N = 0$, the change in sign may be related to fluctuations around 0. We discuss these possibilities in Section 4.2.

3.3 Spatial distribution and heights

The spatial distribution of near-inertial turning depths in the Canadian Basin is nearly uniform at ∼2750 m (Fig. 4, color change from lilac to green at $N^2_{bin} = f^2_\phi$), coinciding with the top of the homogeneous layer or below it (Fig. 5 d–f).

Most of the meridional variability appears to be related to the strength of the stratification and its proximity to topographic slopes. For example, in the region between 72 °N–76.5 °N and > 143 °W, the turning depths occur in a deeper range between 2750–2950 m (Fig. 5a–c) and are located below the top of the homogeneous layer. In this region, N^2_{bin} at 2750 m is relatively large (N^2_{bin} ∼3–5×10^{-8} s^{-2}) compared to the rest of the Canadian Basin at the same depth (N^2_{bin} ∼0. 5–2×10^{-8} s^{-2}), and the top of the homogeneous layer is also deeper than in the eastern Canadian Basin (Fig. 5a and d). Note that these deeper near-inertial turning depths at ∼2850 m are found over nearly flat bathymetry (Fig. 4c), and the latitude varies < 2 ° (Fig. 1, green dots), illustrating that the merid-

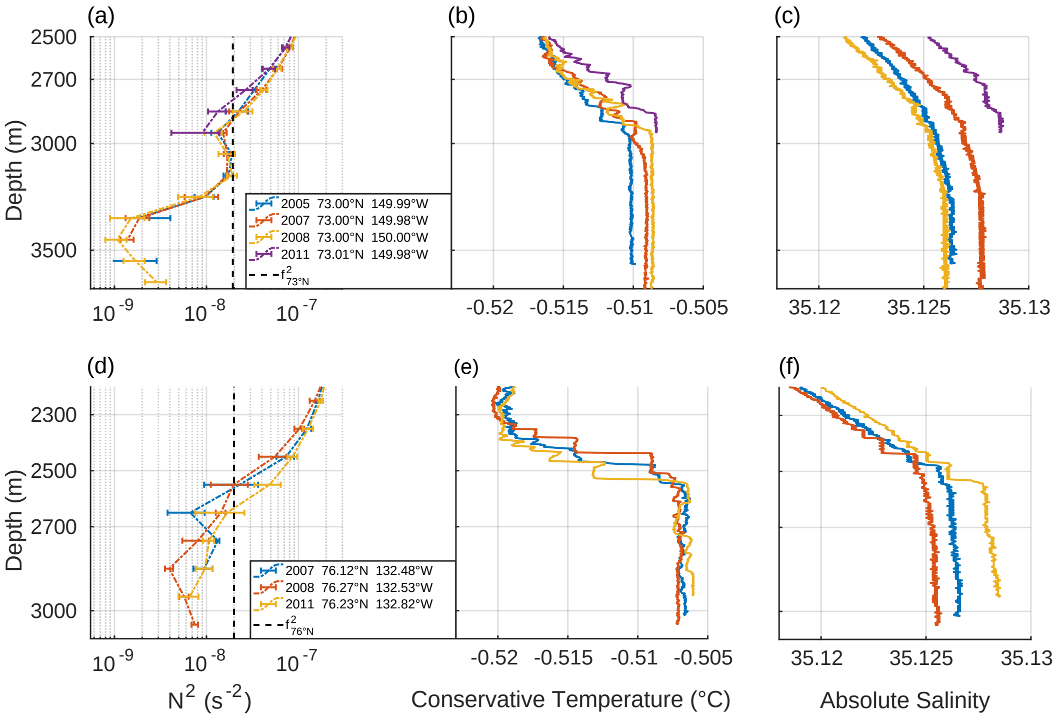

Figure 5. N^2_{bin} and raw Θ and S_A profiles from two small geographic regions between 2005 and 2011. (a–c) Western Canadian Basin at ~73 °N and ~150 °W, (d–f) Eastern Canadian Basin at ~76.2 °N and ~132.5 °W. The vertical lines show the frequencies for $f^2_{73°\mathrm{N}}$ and $f^2_{76°\mathrm{N}}$. In (a) and (d) the horizontal bars are the uncertainties σ_{N^2}. The Θ and S_A profiles show the homogeneous layer and the deep thermohaline staircases. Note that the top and bottom panels have different y-axis limits.

ional variability away from the slope is in part related to the strength of the stratification for latitudes < 76.5 °N.

As N^2_{bin} decreases and f_ϕ increases, the near-inertial turning depths for latitudes > 76. 5 °N remain nearly constant at ~ 2750 m, except in the Marakov Basin, where the near-inertial turning depths are deepest at ~ 3050 m, but have a relatively strong stratification of N^2_{bin} ~1.2–2.8×10 $^{-8}$ s^{-2}, which is compensated by f^2_ϕ.

A peak in N^2_{bin}/f^2_ϕ (light green) below the NiTD at ~3150 m is a consistent feature throughout the Canadian Basin (Fig. 4), coinciding with a slight increase in S_A with depth while Θ remains constant (Fig. 5). Below 3300 m, the stratification is $N^2_{bin} < 0$ within the homogeneous bottom layer (color change from green to blue in Fig. 4), except when S_A or Θ increases with depth. For example, in the deep western Canadian Basin or on the slope in the eastern part (see Fig. 5).

To quantify the proximity to the bathymetry, we defined the turning depth height as the distance from the sea floor to each near-inertial turning depth (Fig. 6). We computed the sea floor depth for each profile by averaging the four nearest depths of the IBCAO bathymetry (Jakobsson et al., 2012) to the profile location.

Generally, the turning depth height distribution is related to the isobaths. Over the slope between the 2500–3500 m isobaths and latitudes < 76 °N, the turning depth heights are between 0–800 m. Below the 3500 m-isobath and over the Canadian abyssal plain, the turning depth heights are between 800–1200 m, increasing northward to a max-

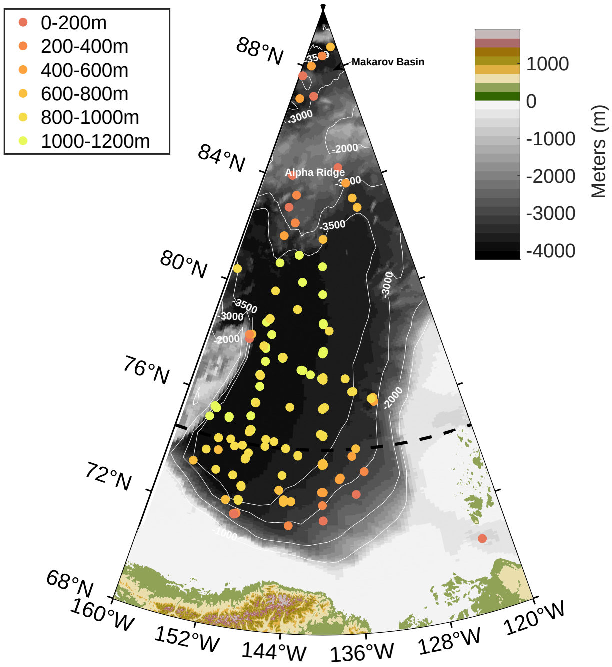

Figure 6. Spatial distribution of turning depth heights in the Canadian Basin. The turning depth height is the distance from the sea floor to each near-inertial turning depth. The black dashed line indicates the critical latitude for the $\omega^2_{M_2}$.

imum of 1000–1200 m. Further northward, on the slope of the Alpha Ridge and the Makarov Basin, the turning depth heights decrease to 0–800 m. Overall, surface-generated NIWs traveling downward are unlikely to interact with the topography since the near-inertial turning depths are far above the seafloor (up to 1000 m). We discuss the possible wave-topography interactions in Section 4.1.

3.4 Non-traditional effects: critical N^2 for NIWs

In stratified hydrostatic geophysical flows, only the vertical component of the Coriolis force is taken into account ($f = 2\Omega \sin(\phi)$). Under these assumptions, the frequency band for internal gravity wave is bounded by f^2 and N^2. Relaxing the hydrostatic approximation to the quasi-hydrostatic approximation, also called non-traditional approximation (NT), involves including the horizontal components of the Coriolis force that vary with the cosine of latitude. With this approximation, the frequency band for internal gravity waves is expanded beyond f^2 and N^2. Among all effects of NT in wave propagation, we are interested in those that happen at depths where $N \approx 0$ and in weakly stratified layers comparable to the Coriolis force $N \approx 2\Omega$. Under NT, a reflection level no longer exists at $\omega = N(z)$ but at a critical buoyancy frequency $\omega = N_{crt}(z)$ typically smaller than the turning depth frequency calculated with the usual traditional approximation (TA) (Gerkema et al., 2008). Explicitly, the critical buoyancy frequency, $N_{crt}(z)$, is defined as follows:

$$N^2_{crit} = \omega^2 \frac{\left(f^2 + f_s^2 - \omega^2\right)}{f^2 - \omega^2} \tag{2}$$

In which $f_s = 2\Omega \cos(\phi) \sin(\alpha)$ is the cosine component of the Coriolis force, and α is the angle to the North-South direction. If we set $\alpha = 0$, the TA definition for a

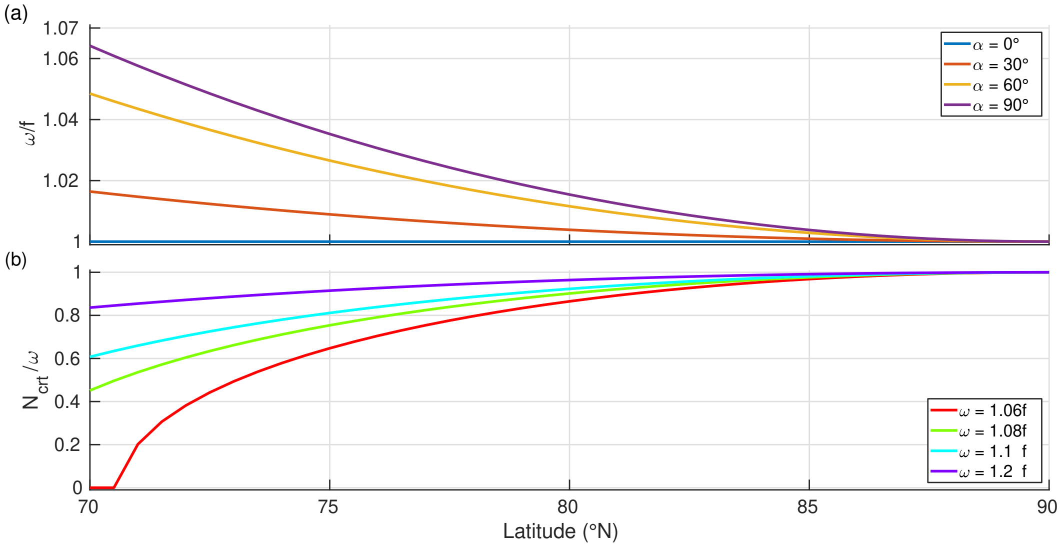

Figure 7. (a) Latitudinal variability of waves with frequency $\omega^2 = f^2 + f_s^2$ normalized by f. Waves with equal and lower frequencies can propagate through arbitrary stratification, and waves with higher frequencies cannot propagate through depths with certain small values of N_{crt}. The colors indicate the direction of propagation, being α the angle to the East-West direction. (b) Example of minimum values of N_{crt}, under NT, for a specific range of waves with near-inertial frequencies and meridional propagation ($\alpha = 90°$), which could be generated at the surface by wind forcing. Waves with these frequencies cannot propagate through depths with these specific values of N_{crt} (normalized by ω).

turning depth is recovered, in which $N(z) = \omega$, and since $f_s = 0$, the wave propagation is purely zonal, implying NT effects act only upon waves propagating with a meridional component (King et al., 2012; Gerkema et al., 2008).

From Eq. 2, we obtain $N_{crit} = 0$ for a wave with frequency $\omega^2 = f^2 + f_s^2$. Waves with this frequency are known as gyroscopic waves, and they can propagate in layers of neutral stratification (van Haren & Millot, 2005), so that there are no turning depth for these waves. In the deep Canadian Basin, near(sub)-inertial fluctuations have been detected (Timmermans et al., 2007), but the nature of the observations suggest these are not gyroscopic waves but that they are related to bottom-trapped topographic Rossby waves at the sub-inertial frequency range (Timmermans et al., 2010; Zhao & Timmermans, 2018).

Note that, since $N_{crit} = 0$ when $\omega^2 = f^2 + f_s^2$, any frequency higher than $f^2 + f_s^2$ result in $N_{crit} > 0$. Thus, the frequency $f^2 + f_s^2$ could be interpreted as the lower limit for a wave to find a turning depth under the NT. For instance, Fig. 7a shows the ω lower limit as a function of f and α. In the Canadian Basin, these frequency values are in the range of $\omega \approx 1 - 1.07 f_\phi$. Pure meridional propagation ($\alpha = 90^\circ$) is associated with the maximum frequencies (lilac line in Fig. 7a), and ω decreases as the wave approach zonal propagation ($\alpha = 0^\circ$).

From Eq. 2 we can estimate N_{crit} for specific near-inertial frequencies that account for hypothetical waves generated at the surface. $\omega = 1.06 - 1.08\,f$ are typical near-inertial frequencies observed in the Arctic Ocean (D'Asaro & Morehead, 1991; Halle, 2003; Fer, 2014; Cole et al., 2018). In general, for latitudes $\geq 72°$ N, near-inertial waves with frequencies $\omega \geq 1.06\,f$ have a turning depth with N_{crit} in the range $0 < N_{crit} \leq f$ in the Canadian Basin (Fig. 7b). Such frequencies N^2_{bin} exist below NiTD at 2750 m in the entire deep Canadian Basin (Section 3.2, Fig. 4). Thus, for both TA and NT, NIWs with $\omega \geq f$ and $\omega \geq 1.06\,f$ have a turning depth up to 1000 m above the sea floor. Under NT, NIWs with frequencies $\omega < 1.06\,f$ traveling meridionally can propagate through arbitrary stratification

4 Discussion

Our results of N^2_{bin} and σ_{N^2} are comparable to previous observations of N^2 in weakly stratified waters. For example, using the method of King et al. (2012), squared buoyancy frequencies lower than the diurnal tidal frequency were found in the South China Sea (Liu et al., 2022) with $N^2_{bin} \approx 5.317 \times 10^{-9}\,\mathrm{s}^{-2}$. This is comparable to the average N^2_{bin} below 3000 m of $\sim 3.1{\times}10^{-9}\,\mathrm{s}^{-2} \pm 2.1{\times}10^{-9}\,\mathrm{s}^{-2}$. Furthermore, squared buoyancy frequencies of $N^2 \sim 4{\times}10^{-8}\,\mathrm{s}^{-2}$ in the deep water of the Canadian Basin (Timmermans et al., 2003; Timmermans & Garrett, 2006) are similar to our average N^2_{bin} below 2500 m of $\sim 1.16 \times 10^{-8}\,\mathrm{s}^{-2} \pm 0.32 \times 10^{-8}\,\mathrm{s}^{-2}$.

In addition, from the WOCE Database typical values of the experimental standard deviation for the semi-diurnal tidal frequency of 0.3–0.1 $\sigma_{\omega_{m2}}$ were computed (King et al., 2012) for the world ocean except for the Arctic Ocean. Along with this, observations of N in the deep Mediterranean Sea were calculated with a standard deviation of $0.8\,f$ over 100 dbar bins; this value was reduced to $0.4\,f$ over 600 dbar bins (van Haren & Millot, 2006). This is similar to the σ_{N^2} values, we found below the NiTD, of $\sigma_{N^2} \leq 0.3\,f^2_\phi$ ($\sigma_N \leq 0.54\,f_\phi$).

The turning depths are related to the location of the deep staircases, the top of the homogeneous layer and the N^2 peak below it (see Fig. 5). For example, taking the top of the homogeneous layer as the depth at which temperature and salinity begin to be constant with depth (e.g. in Fig. 5e–f), Timmermans et al. (2003) reports layer thicknesses of $\sim$1000 m in the central Canadian Basin when the top of the homogeneous layer is at $\sim$2700 m, which is consistent with our definition of NiTD at 2750 m and also with the turning depth height.

The homogeneous layer is deeper in the western Canadian Basin with its upper limit varying meridionally by about 100 m (Timmermans et al., 2007). To the east it is shallower with a thickness of 580 m on the slope at 73.5 °N, 137 °W (Timmermans et al., 2007). In our estimates, the turning depth is deeper to the west (Fig. 4) and the turning depth height to the east is between 400–600 m (Fig. 6). Our results are consistent with the spatial variability of the homogeneous layer thickness (Timmermans et al., 2003; Timmermans & Garrett, 2006). However, in general, the heights of the turning depths are thinner than the thickness of the homogeneous layer, and the near-inertial turning depths are deeper than the top of the homogeneous layer.

4.1 Wave-topography interactions and mixing below a turning depth

For ice-covered oceans, surface-generated internal waves are hypothesized to be partially dissipated under sea ice after one round-trip from the surface to the bottom (Pinkel, 2005; Cole et al., 2018). The NiTD will reduce the distance and travel time of NIWs to reach the surface after reflection, as NIWs cannot propagate through the NiTD. Generally, mixing is low on the flat bottom and increases towards the slopes and ridges (Rainville & Winsor, 2008; Lincoln et al., 2016). In the Canadian Basin, the NiTD overlaps deep slopes and steep topography close to the Alpha Ridge (refer to Fig. 4 and 6), which might prevent waves from playing a more important role in controlling mixing rates above the sea floor.

Even though waves cannot freely propagate across turning depths, part of the wave, known as the evanescent tail, can penetrate. In this process, the wave's amplitude decreases exponentially below the turning depth (Paoletti & Swinney, 2012). In the Canadian Basin, shallow turning depth heights are located above steep and rugged topography (Fig. 6). If those layers are not thick, the evanescent tails of the NIWs can interact with the topography (Paoletti et al., 2014), and they might play a non-trivial role in mixing the Arctic Ocean interior.

From water tank experiments and numerical simulations, Paoletti and Swinney (2012) deduced that the horizontally-integrated vertical energy flux Φ decays exponentially from a turning depth in the following way $\Phi(z) = \Phi_{zc}\ e^{k_c - (z_c - z)}$, in which k_c is the horizontal wave number at the turning depth z_c. From this relation, we can estimate the horizontal wavelength, for which the energy flux $\Phi(z)$ is reduced by an order of magnitude. For turning heights above the bottom in the range of 100-1200 m, such a flux reduction occurs for horizontal wavelengths of 300-3700 m. Therefore, although the energy flux is reduced by an order of magnitude, NIWs at these wavelengths can still interact with the bottom.

The magnitude of k_c at turning depths is unknown. However, assuming the values estimated in section 2.3 and ignoring changes in k as the wave propagates, the flux $\Phi(z)$ of a wave with a horizontal wavelength of 10 km reflecting off a 1200 m thick evanescent layer decreases by a factor of about 2. The reduction of Φ varies with vertical wavelength and frequency range. For example, for $\omega = 1.05f$, shorter or longer initial vertical wavelengths of 10–100 m result in horizontal wavelengths of ∼1.8–18.8 km and a reduction in wave flux by a factor of ∼65–1.5. Similarly, for a fixed vertical wavelength of 50 m, a change in ω between $1.01f$ and $1.1f$ results in a horizontal wavelength of ∼7–2 km and a reduction in wave flux by a factor of ∼ 1.4–3. In particular, significant reductions in wave flux occur only for internal waves with horizontal wavelengths < 5000 m at turning depths.

Wave-topography interactions below a turning depth have been studied using numerical models and water tank experiments. For example, topography below a turning depth can generate internal tides under tidal forcing (Paoletti et al., 2014), and evanescent wave perturbations can generate propagating waves after reaching a depth where $\omega < N^2(z)$ (Lee et al., 2020). Thus, despite the presence of NiTDs, NIWs can still partially account for the deep mixing in the Canadian Basin.

At the top of the homogeneous layer there are thermohaline staircases with a step size of ∼ 10–50 m and a transition layer of ∼ 10–25 m throughout the Canadian Basin (Timmermans et al., 2003, 2010; Zhou & Lu, 2013; Zhou et al., 2014). These density structures act as a filter for internal waves (Ghaemsaidi et al., 2016; Sutherland, 2016), leading to wave reflection especially for waves with relatively short length scales. The vertical location of the staircases varies, but assuming that the staircases are between 2500–2700 m (see Fig. 5), then $N^2_{bin} \sim$ 2–9$\times10^{-8}\,\mathrm{s}^{-2}\pm$ 1–2$\times10^{-8}\,\mathrm{s}^{-2}$. However, between each step, the stratification is close to zero ($N \sim 0$), which cannot be accurately represented by averaging over 100–meter bins. As a result, the binned N^2_{bin} fails to reproduce the step-wise stratification with $N \sim 0$ between steps.

We expected that surface-generated near-inertial waves interact with the staircases before reaching the NiTD, modifying their propagation depending on the time and length scales of the wave (Ghaemsaidi et al., 2016). For typical values of mid-water stair-cases and internal waves in the Arctic Ocean, NIWs with wavelength of approximately 50 km transmit across the staircases with little reflection (Sutherland, 2016). These NIWs can continue to propagate downwards, but for the staircases in the deep abyss, the internal waves immediately encounter the homogeneous bottom layer and the bottom itself. For this case, let us assume a stratification that allows internal waves to propagate across the deep staircases. We can then calculate the lower wavelength limit of the transmitting waves $\lambda_{Tl} \simeq 0.5\pi D\,(\,0.1\,(\omega^2 - f^2\,)/\,N^2)^{-1/2}$ (Sutherland, 2016), where D is the total length of the staircase. For $\omega = 1.05f$, $D = 150\,\mathrm{m}$ and $f = 0.5N$ (N_{bin} between 2500–2700 m), the lower bound for internal waves transmitting with little reflection is $\lambda_{Tl} \simeq 4.6\,\mathrm{km}$. Therefore, we would expect NIWs with longer wavelengths to be able to propagate. However, we cannot rule out other processes, in which NIWs attenuate or promote mixing, such as the onset of instability within the staircase.

4.2 Unstable layers and convective instability

If the main impact of the NiTD in the deep Canadian Basin is to isolate the bottom from surface-generated wind-driven waves, NIWs will not play a substantial role in driving the bottom layer dynamics, and other processes, for example, convective instability, govern bottom mixing.

Geothermal heat flux estimates in the Canadian Basin are $F_H \sim 40{-}60\ \ \mathrm{mW\,m^{-2}}$ (Langseth et al., 1990). A considerable fraction of this heat remains in the homogeneous bottom layer. Approximately $F_H \sim 0.1 - 45\ \ \mathrm{mW\,m^{-2}}$ escape through density staircases above the bottom layer (Carmack et al., 2012; Zhou & Lu, 2013; Zhou et al., 2014; Timmermans et al., 2003).

There are two main hypotheses for driving this heat flux transport. The heat is transported either horizontally and escapes near the slope where mixing is strong (Timmermans et al., 2003), or it is driven vertically by thermobaric convection (Carmack et al., 2012). There is evidence that convective instability controls the bottom layer (Zhou et al., 2014) supporting the direct vertical flux of heat. Between 3300–3900 m, we identified consecutive locally unstable layers, which also supports the convective instability hypothesis.

The geothermal flux heats the layer from below, which increases the temperature of the adjacent water parcels. This layer gains buoyancy and destabilizes the upper layers, which may be reflected in the alternating positive and negative N^2_{bin} values. We expect that the homogeneous layer is close to neutral buoyancy $N \approx 0$, but finding exact values of $N = 0$ is unrealistic. The locally unstable values of N^2_{bin} might be related to fluctuations around $N^2_{bin} = 0$, so that the layer does have neutral buoyancy but is unstable, suggesting periods of convective mixing. In addition, the homogeneous layer may have a theoretical thickness of 1051 m (Zhou et al., 2014) based on a comparison of the deep Canadian homogeneous layer thickness to experiments conducted with salt-stratified fluids heated from below. If we consider only the unstable layers (Figs. 3 and 4), the thickness of the homogeneous layer is $\sim 600 - 700\,\mathrm{m}$. However, assuming that the top of the homogeneous layer is at $\sim$3000 m, just above the peak in N^2_{bin} (Fig. 3), the thickness increases up to 1000 m, which is consistent with Zhou et al. (2014) and therefore with the convective instability hypothesis.

In the ocean, NIW-driven near-bottom dissipation is still largely unknown (Thomas & Zhai, 2022). We cannot directly compare the results obtained by experiments and simulations described in this section to the actual ocean. However, our results show that in the Arctic Ocean, near-inertial turning depths exist and may play a bigger role in the propagation and reflection of NIWs than elsewhere. Further study is needed to understand the wave dynamics in the changing Arctic Ocean. Finally, a homogeneous bottom layer is also present in the Eurasian Basin, and the analysis of some profiles shows turning depths for NIWs (not shown). Hence some of the impacts and effects discussed in this section might also apply to the Eurasian Basin.

5 Summary & Conclusion

Our analyses of buoyancy frequency N^2 in the deep Canadian Basin and interpretations of near-inertial turning depths are summarized as follows:

1. From the analysis of N^2_{bin} derived from temperature and salinity profiles of the UDASH dataset from 2005 to 2014 and a statistical method of King et al. (2012), near-inertial turning depths are found in the deep Canadian Basin at $\sim$2750 m depth and between 100 m and 1200 m above the sea floor.
2. For the traditional and the non-traditional approximation, NIWs have turning depths for frequencies $\omega \geq f_\phi$ and $\omega \geq 1.06 f_\phi$, respectively. Furthermore, under the non-traditional approximation, NIWs with frequencies $\omega < 1.06 f_\phi$ traveling meridionally can propagate through arbitrary stratification.
3. There are layers below 3300 m that are locally slightly unstable, $N^2_{bin} < 0$. These values are consistent with a homogeneous layer that is quasi-neutral with $N \approx 0$, and with the hypothesis that geothermal flux heats the homogeneous bottom layer from below, destabilizing the overlying layers.
4. After reflection at the NiTD the evanescent wave tails may interact with bathymetry, mainly over slopes where the turning-depth heights above topography are small.

The evidence presented in this study cannot prove with certainty that NIWs reflect at turning depths in the deep Canadian Basin. However, we provided different scenarios involving near-inertial wave reflection from turning depths. Further measurements, numerical simulations, and theory are necessary to understand the interaction of near-inertial waves upon reflection from turning depths and to link surface-generated waves to mixing rates in the interior and above slopes in the Canadian Basin. This understanding may become very important for correctly representing the changing Arctic Ocean and its future state in climate projections.

Acknowledgments

This research was carried out within the International Research Training Group ArcTrain: “Processes and impacts of climate change in the North Atlantic Ocean and the Canadian Arctic” (IRTG 1904 ArcTrain), and it was funded by the Deutsche Forschungsgemeinschaft (DFG, German Research Foundation).

Further, this paper is a contribution to projects T3 and W5 of the Collaborative Research Centre TRR 181 ”Energy Transfer in Atmosphere and Ocean” (project number 274762653) and to the project C04 of the Transregional Collaborative Research Center “ArctiC Amplification: Climate Relevant Atmospheric and SurfaCe Processes, and Feedback Mechanisms (AC)^3 (Project number 268020496) funded by the DFG.

The majority of the CTD profiles of the UDASH database that were selected for this study were collected during the Joint Ocean Ice Study (JOIS) program (http://www.whoi.edu/beaufortgyre/)

The authors would like to thank the anonymous reviewer for his helpful comments, which have improved the quality of the manuscript.

6 Open Research

Data - The data set containing temperature and salinity used in this study (Behrendt et al., 2017) is stored in PANGAEA-Data Publisher for Earth & Environmental Science, and it can be found at DOI: `https://doi.org/10.1594/PANGAEA.872931`. The bathymetric data (Jakobsson et al., 2012) can be found at `https://www.ngdc.noaa.gov/mgg/bathymetry/arctic/ibcaoversion3.html`.

References

Behrendt, A., Sumata, H., Rabe, B., & Schauer, U. (2017). *A comprehensive, quality-controlled and up-to-date data set of temperature and salinity data* *for the Arctic Mediterranean Sea (Version 1.0), links to data files* [Data]. PANGAEA. Retrieved from https://doi.org/10.1594/PANGAEA.872931 (Supplement to: Behrendt, A et al. (2017): UDASH - Unified Database for Arctic and Subarctic Hydrography. Earth System Science Data Discussions, 37 pp, https://doi.org/10.5194/essd-2017-92) doi: 10.1594/PANGAEA.872931

Behrendt, A., Sumata, H., Rabe, B., & Schauer, U. (2018, June). UDASH – Unified Database for Arctic and Subarctic Hydrography [Data]. *Earth System Science Data*, *10*(2), 1119–1138. Retrieved 2022-09-01, from https://essd.copernicus.org/articles/10/1119/2018/ doi: 10.5194/essd-10-1119-2018

Carmack, E. C., Williams, W. J., Zimmermann, S. L., & McLaughlin, F. A. (2012, April). The Arctic Ocean warms from below: THE ARCTIC OCEAN WARMS FROM BELOW. *Geophysical Research Letters*, *39*(7), n/a–n/a. Retrieved 2022-11-15, from http://doi.wiley.com/10.1029/2012GL050890 doi: 10.1029/2012GL050890

Cole, S. T., Toole, J. M., Rainville, L., & Lee, C. M. (2018, August). Internal Waves in the Arctic: Influence of Ice Concentration, Ice Roughness, and Surface Layer Stratification. *Journal of Geophysical Research: Oceans*, *123*(8), 5571–5586. Retrieved 2022-09-16, from https://onlinelibrary.wiley.com/doi/abs/10.1029/2018JC014096 doi: 10.1029/2018JC014096

D'Asaro, E. A., & Morehead, M. D. (1991). Internal waves and velocity fine structure in the Arctic Ocean. *Journal of Geophysical Research*, *96*(C7), 12725. Retrieved 2022-09-16, from http://doi.wiley.com/10.1029/91JC01071 doi: 10.1029/91JC01071

Dosser, H. V., & Rainville, L. (2016, February). Dynamics of the Changing Near-Inertial Internal Wave Field in the Arctic Ocean. *Journal of Physical Oceanography*, *46*(2), 395–415. Retrieved 2022-12-08, from https://journals.ametsoc.org/view/journals/phoc/46/2/jpo-d-15-0056.1.xml doi: 10.1175/JPO-D-15-0056.1

Dosser, H. V., Rainville, L., & Toole, J. M. (2014, February). Near-Inertial Internal Wave Field in the Canada Basin from Ice-Tethered Profilers. *Journal of Physical Oceanography*, *44*(2), 413–426. Retrieved 2022-12-06, from http://journals.ametsoc.org/doi/10.1175/JPO-D-13-0117.1 doi: 10.1175/JPO-D-13-0117.1

Fer, I. (2014, August). Near-Inertial Mixing in the Central Arctic Ocean. *Journal of Physical Oceanography*, *44*(8), 2031–2049. Retrieved 2022-09-01, from http://journals.ametsoc.org/doi/10.1175/JPO-D-13-0133.1 doi: 10.1175/JPO-D-13-0133.1

Fine, E. C., & Cole, S. T. (2022, May). Decadal Observations of Internal Wave Energy, Shear, and Mixing in the Western Arctic Ocean. *Journal of Geophysical Research: Oceans*, *127*(5). Retrieved 2022-12-08, from https://onlinelibrary.wiley.com/doi/10.1029/2021JC018056 doi: 10.1029/2021JC018056

Gerkema, T., Zimmerman, J. T. F., Maas, L. R. M., & van Haren, H. (2008, May). Geophysical and astrophysical fluid dynamics beyond the traditional approximation. *Reviews of Geophysics*, *46*(2), RG2004. Retrieved 2022-09-29, from http://doi.wiley.com/10.1029/2006RG000220 doi: 10.1029/2006RG000220

Ghaemsaidi, S. J., Dosser, H. V., Rainville, L., & Peacock, T. (2016, February). The impact of multiple layering on internal wave transmission. *Journal of Fluid Mechanics*, *789*, 617–629. Retrieved 2022-09-16, from https://www.cambridge.org/core/product/identifier/S0022112015006825/type/journal_article doi: 10.1017/jfm.2015.682

Gregg, M. C. (2021). *Ocean Mixing* (1st ed.). Cambridge University Press. Retrieved 2022-12-06, from https://www.cambridge.org/core/product/

identifier/9781316795439/type/book doi: 10.1017/9781316795439
Halle, C. (2003). Internal wave variability in the Beaufort Sea during the winter of 1993/1994. *Journal of Geophysical Research*, *108*(C7), 3210. Retrieved 2022-09-16, from http://doi.wiley.com/10.1029/2000JC000703 doi: 10.1029/2000JC000703

Jakobsson, M., Mayer, L., Coakley, B., Dowdeswell, J. A., Forbes, S., Fridman, B., … Weatherall, P. (2012, June). The International Bathymetric Chart of the Arctic Ocean (IBCAO) Version 3.0: IBCAO VERSION 3.0 [Data]. *Geophysical Research Letters*, *39*(12), n/a–n/a. Retrieved 2022-09-01, from http://doi.wiley.com/10.1029/2012GL052219 doi: 10.1029/2012GL052219

Kim, Y.-H., Min, S.-K., Gillett, N. P., Notz, D., & Malinina, E. (2023, June). Observationally-constrained projections of an ice-free Arctic even under a low emission scenario. *Nature Communications*, *14*(1), 3139. Retrieved 2023-06-11, from https://www.nature.com/articles/s41467-023-38511-8 doi: 10.1038/s41467-023-38511-8

King, B., Stone, M., Zhang, H. P., Gerkema, T., Marder, M., Scott, R. B., & Swinney, H. L. (2012, April). Buoyancy frequency profiles and internal semidiurnal tide turning depths in the oceans: INTERNAL TIDE TURNING DEPTH. *Journal of Geophysical Research: Oceans*, *117*(C4), n/a–n/a. Retrieved 2022-09-01, from http://doi.wiley.com/10.1029/2011JC007681 doi: 10.1029/2011JC007681

Kwok, R. (2018, October). Arctic sea ice thickness, volume, and multiyear ice coverage: losses and coupled variability (1958–2018). *Environmental Research Letters*, *13*(10), 105005. Retrieved 2023-06-11, from https://iopscience.iop.org/article/10.1088/1748-9326/aae3ec doi: 10.1088/1748-9326/aae3ec

Langseth, M. G., Lachenbruch, A. H., & Marshall, B. V. (1990). Geothermal observations in the Arctic region. In A. Grantz, L. Johnson, & J. F. Sweeney (Eds.), *The Arctic Ocean Region* (pp. 133–151). United Sates: Geological Society of America. Retrieved 2022-11-16, from https://pubs.geoscienceworld.org/books/book/866/chapter/4862450/ doi: 10.1130/DNAG-GNA-L.133

Lee, A., Hakes, K., Liu, Y., Allshouse, M. R., & Crockett, J. (2020, December). Evanescent to propagating internal waves in experiments, simulations, and linear theory. *Experiments in Fluids*, *61*(12), 252. Retrieved 2022-11-17, from http://link.springer.com/10.1007/s00348-020-03077-4 doi: 10.1007/s00348-020-03077-4

Lenn, Y.-D., Fer, I., Timmermans, M.-L., & MacKinnon, J. A. (2022). Mixing in the Arctic Ocean. In *Ocean Mixing* (pp. 275–299). Elsevier. Retrieved 2022-11-09, from https://linkinghub.elsevier.com/retrieve/pii/B9780128215128000189 doi: 10.1016/B978-0-12-821512-8.00018-9

Lincoln, B. J., Rippeth, T. P., Lenn, Y.-D., Timmermans, M. L., Williams, W. J., & Bacon, S. (2016, September). Wind-driven mixing at intermediate depths in an ice-free Arctic Ocean. *Geophysical Research Letters*, *43*(18), 9749–9756. doi: 10.1002/2016GL070454

Liu, K., Da, L., Guo, W., Liu, C., & Sun, J. (2022, February). Turning depths of internal tides in the South China Sea inferred from profile data. *Acta Oceanologica Sinica*, *41*(2), 139–146. Retrieved 2022-09-01, from https://link.springer.com/10.1007/s13131-021-1837-8 doi: 10.1007/s13131-021-1837-8

McDougall, T. J., & Barker, P. M. (2011). *Getting started with TEOS-10 and the Gibbs Seawater (GSW) Oceanographic Toolbox.* Battery Point, Tas.: Trevor J McDougall. (OCLC: 724024071)

McDougall, T. J., & Barker, P. M. (2014, December). Comment on "Buoyancy frequency profiles and internal semidiurnal tide turning depths in the oceans" by

B. King et al. *Journal of Geophysical Research: Oceans*, *119*(12), 9026–9032. Retrieved 2022-09-06, from http://doi.wiley.com/10.1002/2014JC010066 doi: 10.1002/2014JC010066

Meyer, A., Fer, I., Sundfjord, A., & Peterson, A. K. (2017, June). Mixing rates and vertical heat fluxes north of Svalbard from Arctic winter to spring: N-ICE2015 ARCTIC TURBULENCE OBSERVATIONS. *Journal of Geophysical Research: Oceans*, *122*(6), 4569–4586. Retrieved 2022-12-08, from http://doi.wiley.com/10.1002/2016JC012441 doi: 10.1002/2016JC012441

Morison, J. H., Long, C. E., & Levine, M. D. (1985, November). Internal wave dissipation under sea ice. *Journal of Geophysical Research: Oceans*, *90*(C6), 11959–11966. doi: 10.1029/JC090iC06p11959

Nurser, A. J. G., & Bacon, S. (2014, November). The Rossby radius in the Arctic Ocean. *Ocean Science*, *10*(6), 967–975. Retrieved 2022-09-01, from https://os.copernicus.org/articles/10/967/2014/ doi: 10.5194/os-10-967-2014

Olbers, D. J. (2012). *Ocean dynamics* (First edition ed.). Heidelberg ; New York: Springer.

Paoletti, M. S., Drake, M., & Swinney, H. L. (2014, March). Internal tide generation in nonuniformly stratified deep oceans. *Journal of Geophysical Research: Oceans*, *119*(3), 1943–1956. Retrieved 2022-11-17, from http://doi.wiley.com/10.1002/2013JC009469 doi: 10.1002/2013JC009469

Paoletti, M. S., & Swinney, H. L. (2012, September). Propagating and evanescent internal waves in a deep ocean model. *Journal of Fluid Mechanics*, *706*, 571–583. Retrieved 2022-11-13, from https://www.cambridge.org/core/product/identifier/S0022112012002844/type/journal_article doi: 10.1017/jfm.2012.284

Peterson, A. K., Fer, I., McPhee, M. G., & Randelhoff, A. (2017, February). Turbulent heat and momentum fluxes in the upper ocean under Arctic sea ice: TURBULENT FLUXES UNDER ARCTIC SEA ICE. *Journal of Geophysical Research: Oceans*, *122*(2), 1439–1456. Retrieved 2022-12-08, from http://doi.wiley.com/10.1002/2016JC012283 doi: 10.1002/2016JC012283

Pinkel, R. (2005, May). Near-Inertial Wave Propagation in the Western Arctic. *Journal of Physical Oceanography*, *35*(5), 645–665. Retrieved 2022-09-16, from http://journals.ametsoc.org/doi/10.1175/JPO2715.1 doi: 10.1175/JPO2715.1

Rainville, L., Lee, C., & Woodgate, R. (2011, September). Impact of Wind-Driven Mixing in the Arctic Ocean. *Oceanography*, *24*(3), 136–145. Retrieved 2022-12-08, from https://tos.org/oceanography/article/impact-of-wind-driven-mixing-in-the-arctic-ocean doi: 10.5670/oceanog.2011.65

Rainville, L., & Winsor, P. (2008, April). Mixing across the Arctic Ocean: Microstructure observations during the Beringia 2005 Expedition. *Geophysical Research Letters*, *35*(8), L08606. Retrieved 2022-11-09, from http://doi.wiley.com/10.1029/2008GL033532 doi: 10.1029/2008GL033532

Rainville, L., & Woodgate, R. A. (2009, December). Observations of internal wave generation in the seasonally ice-free Arctic. *Geophysical Research Letters*, *36*(23), L23604. Retrieved 2022-12-07, from http://doi.wiley.com/10.1029/2009GL041291 doi: 10.1029/2009GL041291

Rippeth, T. P., Vlasenko, V., Stashchuk, N., Scannell, B. D., Green, J. A. M., Lincoln, B. J., & Bacon, S. (2017, December). Tidal Conversion and Mixing Poleward of the Critical Latitude (an Arctic Case Study). *Geophysical Research Letters*, *44*(24). Retrieved 2022-09-07, from https://onlinelibrary.wiley.com/doi/10.1002/2017GL075310 doi: 10.1002/2017GL075310

Sutherland, B. R. (2010). *Internal gravity waves*. Cambridge ; New York: Cambridge University Press. (OCLC: ocn601113971)

Sutherland, B. R. (2016, May). Internal wave transmission through a thermohaline staircase. *Physical Review Fluids*, *1*(1), 013701. doi: 10.1103/PhysRevFluids.1

.013701
Thomas, L. N., & Zhai, X. (2022). The lifecycle of surface-generated near-inertial waves. In *Ocean Mixing* (pp. 95–115). Elsevier. Retrieved 2022-09-16, from https://linkinghub.elsevier.com/retrieve/pii/B9780128215128000128 doi: 10.1016/B978-0-12-821512-8.00012-8

Timmermans, M.-L., & Garrett, C. (2006, May). Evolution of the Deep Water in the Canadian Basin in the Arctic Ocean. *Journal of Physical Oceanography*, *36*(5), 866–874. Retrieved 2022-09-06, from http://journals.ametsoc.org/doi/10.1175/JPO2906.1 doi: 10.1175/JPO2906.1

Timmermans, M.-L., Garrett, C., & Carmack, E. (2003, October). The thermohaline structure and evolution of the deep waters in the Canada Basin, Arctic Ocean. *Deep Sea Research Part I: Oceanographic Research Papers*, *50*(10-11), 1305–1321. Retrieved 2022-09-06, from https://linkinghub.elsevier.com/retrieve/pii/S0967063703001250 doi: 10.1016/S0967-0637(03)00125-0

Timmermans, M.-L., Melling, H., & Rainville, L. (2007, April). Dynamics in the Deep Canada Basin, Arctic Ocean, Inferred by Thermistor Chain Time Series. *Journal of Physical Oceanography*, *37*(4), 1066–1076. Retrieved 2022-09-01, from http://journals.ametsoc.org/doi/10.1175/JPO3032.1 doi: 10.1175/JPO3032.1

Timmermans, M.-L., Rainville, L., Thomas, L., & Proshutinsky, A. (2010, May). Moored observations of bottom-intensified motions in the deep Canada Basin, Arctic Ocean. *Journal of Marine Research*, *68*(3), 625–641. Retrieved 2022-09-01, from http://www.ingentaconnect.com/content/10.1357/002224010794657137 doi: 10.1357/002224010794657137

van Haren, H., & Millot, C. (2005). Gyroscopic waves in the Mediterranean Sea. *Geophysical Research Letters*, *32*(24), L24614. Retrieved 2022-09-16, from http://doi.wiley.com/10.1029/2005GL023915 doi: 10.1029/2005GL023915

van Haren, H., & Millot, C. (2006). Determination of buoyancy frequency in weakly stable waters. *Journal of Geophysical Research*, *111*(C3), C03014. Retrieved 2022-09-01, from http://doi.wiley.com/10.1029/2005JC003065 doi: 10.1029/2005JC003065

Vlasenko, V., Stashchuk, N., Hutter, K., & Sabinin, K. (2003, March). Nonlinear internal waves forced by tides near the critical latitude. *Deep Sea Research Part I: Oceanographic Research Papers*, *50*(3), 317–338. Retrieved 2023-06-08, from https://linkinghub.elsevier.com/retrieve/pii/S0967063703000189 doi: 10.1016/S0967-0637(03)00018-9

Walsh, J. E., Fetterer, F., Scott Stewart, J., & Chapman, W. L. (2017, January). A database for depicting Arctic sea ice variations back to 1850. *Geographical Review*, *107*(1), 89–107. Retrieved 2023-06-11, from https://www.tandfonline.com/doi/full/10.1111/j.1931-0846.2016.12195.x doi: 10.1111/j.1931-0846.2016.12195.x

Zhao, B., & Timmermans, M. (2018, September). Topographic Rossby Waves in the Arctic Ocean's Beaufort Gyre. *Journal of Geophysical Research: Oceans*, *123*(9), 6521–6530. Retrieved 2022-09-29, from https://onlinelibrary.wiley.com/doi/10.1029/2018JC014233 doi: 10.1029/2018JC014233

Zhou, S.-Q., & Lu, Y.-Z. (2013, December). Characterization of double diffusive convection steps and heat budget in the deep Arctic Ocean: DDC and Heat Budget in the Deep Arctic. *Journal of Geophysical Research: Oceans*, *118*(12), 6672–6686. Retrieved 2022-11-15, from http://doi.wiley.com/10.1002/2013JC009141 doi: 10.1002/2013JC009141

Zhou, S.-Q., Qu, L., Lu, Y.-Z., & Song, X.-L. (2014, February). The instability of diffusive convection and its implication for the thermohaline staircases in the deep Arctic Ocean. *Ocean Science*, *10*(1), 127–134. Retrieved 2022-11-15, from https://os.copernicus.org/articles/10/127/2014/ doi:

10.5194/os-10-127-2014